Astroparticle Physics 175 (2026) 103170

Contents lists available at ScienceDirect

Astroparticle Physics

journal homepage: www.elsevier.com/locate/astropartphys

Measurement of the re-entrant all-electron spectrum by the High-Energy Particle Detector on board the China Seismo-Electromagnetic Satellite

S. Amoroso [a,b], M. Babu [c,d], S. Bartocci [e], R. Battiston [c,d], S. Beolè [f,g], W.J. Burger [d], D. Campana [h], P. Cipollone [b], L. Conti [b,i,q], A. Contin [j,k], M. Cristoforetti [l,d], C. De Donato [b], C. De Santis [b], A. Di Luca [l,d], F.M. Follega [c,d], G. Gebbia [c,d], R. Iuppa [c,d], A. Lega [c,d], M. Lolli [k], M. Martucci [b], G. Masciantonio [b], M. Mergè [m], M. Mese [n,h], C. Neubüser [d], R. Nicolaidis [c,d], F. Nozzoli [d], A. Oliva [k], G. Osteria [h], F. Palma [b], B. Panico [n,h], F. Perfetto [h], A. Perinelli [c,d], P. Picozza [a,b], S. Pietroni [a,b], M. Pozzato [k], E. Ricci [c,d], L. Ricci [c,d], M. Ricci [b,o], S.B. Ricciarini [p], Z. Sahnoun [j,k], U. Savino [f,g], V. Scotti [n,h], M. Sorbara [a,b,*], A. Sotgiu [b], R. Sparvoli [a,b], P. Ubertini [q], V. Vilona [d], S. Zoffoli [m], P. Zuccon [c,d]

[a] Università di Roma Tor Vergata, V. della Ricerca Scientifica 1, 00133, Roma, Italy
[b] INFN - Sezione di Roma Tor Vergata, V. della Ricerca Scientifica 1, 00133, Roma, Italy
[c] Università di Trento, V. Sommarive 14, 38123 Povo (TN), Italy
[d] INFN - TIFPA, V. Sommarive 14, 38123 Povo (TN), Italy
[e] INFN - AC, V. E. Fermi 54, 00044 Frascati (RM), Italy
[f] Università di Torino, V. P. Giuria 1, 10125, Torino, Italy
[g] INFN - Sezione di Torino, V. P. Giuria 1, 10125, Torino, Italy
[h] INFN - Sezione di Napoli, V. Cintia, 80126, Napoli, Italy
[i] Uninettuno University, C.so V. Emanuele II, 39, I-00186, Rome, Italy
[j] Università di Bologna, V.le Berti Pichat 6/2, 40127, Bologna, Italy
[k] INFN - Sezione di Bologna, V.le Berti Pichat 6/2, 40127, Bologna, Italy
[l] Fondazione Bruno Kessler, V. Sommarive 18, 38123, Povo (TN), Italy
[m] Italian Space Agency, V. del Politecnico, 00133 Roma, Italy
[n] Università degli Studi di Napoli Federico II, V. Cintia, 80126, Napoli, Italy
[o] INFN - LNF, V. E. Fermi 54, 00044 Frascati (RM), Italy
[p] IFAC - CNR, V. Madonna del Piano 10, 50019 Sesto Fiorentino (FI), Italy
[q] INAF - IAPS, V. Fosso del Cavaliere 100, 00133, Roma, Italy

ARTICLE INFO

Keywords:
Cosmic-Rays
Magnetosphere
Albedo electrons
Calorimeter

ABSTRACT

Interactions of primary cosmic rays with residual atmospheric nuclei produce secondary leptons through the decay chain of short-lived pions. Even though generated with an upward direction, a fraction of these secondary electrons and positrons is bent back downward towards the Earth by the geomagnetic field lines (hence they are called re-entrant albedo). In this paper, we report on a new measurement of the re-entrant all-electron differential flux in the energy range 10-100 MeV, performed by the High-Energy Particle Detector (HEPD-01) on board the China Seismo-Electromagnetic Satellite (CSES-01) in the near-equatorial region at about 500 km altitude between 2018 and 2022. This analysis focuses on the re-entrant all-electron spectrum that covers the low energy interval in a geographical region characterized by a substantial lack of recent experimental data and can contribute to a more accurate definition of secondary electron and positron population distribution and refine the radiation models in the Earth's magnetosphere.

1. Introduction

Primary galactic particles can penetrate the Earth's magnetic field and interact with nuclei in the outermost layers of the atmosphere, thus producing secondary particles. A certain amount of these secondaries move upward along the field line (the so-called splash albedo particles) and, if their rigidity exceeds the local geomagnetic cutoff, they can

* Corresponding author at: Università di Roma Tor Vergata, V. della Ricerca Scientifica 1, 00133, Roma, Italy.
E-mail address: matteo.sorbara@roma2.infn.it (M. Sorbara).

https://doi.org/10.1016/j.astropartphys.2025.103170
Received 14 May 2025; Received in revised form 18 August 2025; Accepted 20 August 2025
Available online 1 September 2025

escape towards the interplanetary space. Conversely, if these particles lack the momentum to penetrate into the atmosphere (i.e. if they present a rigidity below the geomagnetic cutoff) they can be trapped by the geomagnetic field in closed-loop orbits and re-enter in the opposite hemisphere with a downward direction (hence the name re-entrant albedo particles). In Treiman [1] it was first shown that the re-entrant albedo particles arrive at latitudes very close to the latitude from which they left the Earth, although the longitude is generally changed. Due to a whole set of experimental data since the 1950s, it is known that electrons, positrons and protons are the dominating components of albedo particles, but light nuclei are also present. These particles were first studied with several balloon-borne instruments during the second half of the last century [2–6]. However, many of these experiments suffered from some limitations, such as the large background due to atmospheric particles or the limited geographical coverage observable with a balloon-borne experiment. With the advent of spacecraft missions, it became possible to measure the differential energy spectrum of albedo particles in various regions of the near-Earth space.

As for the all-electron component of albedo particles, secondary electrons and positrons are produced through the decay chains ($\pi^{\pm} \rightarrow \mu^{\pm} \rightarrow e^{\pm}$) of the short-lived pions coming from the interactions of primary cosmic rays with nuclei in the residual atmosphere. Depending on the primary proton energy, the cross-section for π^{+} production is up to two times greater than for π^{-}, and so positrons are expected to dominate [7]. The secondary positron to electron flux ratio depends on effects related to primary propagation as well as the motion of trapped particles along the geomagnetic field lines. Secondaries are largely produced by positively charged primaries (mainly protons and helium nuclei) arriving from the West, and move in the same direction as the primary. Once moving along the geomagnetic field lines, secondary electrons will gyrate clockwise towards the Earth and interact with the atmosphere, before being detected by the orbiting apparatus. Secondary positrons will gyrate anti-clockwise, reaching higher altitudes before moving towards the Earth's atmosphere. These two East–West asymmetries generate a positron excess with a magnitude depending on the geomagnetic location, as observed first by MARIYA-2 [8] on board the Mir station and AMS-01 [9,10] on the Space Shuttle Discovery and then by the satellite-borne experiment PAMELA [7,11]. More recently, the spectra of re-entrant albedo electrons and positrons at the top of the atmosphere were also measured by the balloon-borne spectrometer AESOP-Lite [12]. However, a direct comparison with the results presented in this paper is not feasible, since the geographical coverage of the balloon experiment is not compatible with the L-shell selection applied in this measurement. These secondary electron and positron fluxes have a complex spatial structure due to their interactions with, and motion in, the geomagnetic field, the energy dependence of the production cross-sections and the atmospheric absorption of produced particles. A dependence on the daytime/nightime portion of the orbit was also suggested in [13] due to the different flow of the solar wind and its interaction with the Earth magnetosphere. Even though these processes are well known, theoretical models (e.g., [14,15]) are not always able to adequately reproduce the experimental results.

In this work, the re-entrant electrons and positrons spectrum measured by the High-Energy Particle Detector (HEPD-01) – orbiting on board the China Seismo-Electromagnetic Satellite (CSES-01) – is presented at energies between 10 and 100 MeV, in a geographical region where recent data are lacking, and compared with complementary measurements by the PAMELA experiment. These results complete our previous work on the measurements of low-energy, re-entrant albedo protons [16] and anticipate those by HEPD-01's improved successor, HEPD-02 [17], launched on June 14th 2025 on board the CSES-02 satellite. Since the HEPD-01 detector cannot distinguish between a particle charge, electrons and positrons cannot be discriminated one another. The term all-electrons will be used from now on to describe both electrons and positrons.

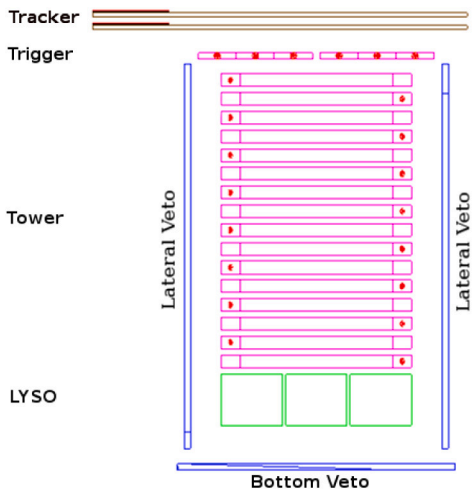

Fig. 1. Schematic view of the HEPD-01 detector. See text for details on the subsystems.

2. The HEPD-01 detector on board the CSES-01 satellite

The CSES-01 satellite [18] was launched on February 2, 2018 as the first of an extended constellation of Low-Earth Orbit (LEO) satellites, designed for monitoring perturbations of electromagnetic fields, waves, plasma and charged particle fluxes, either due to natural (earthquakes, solar events, cosmic rays, etc.) or anthropogenic sources in the near-Earth space. In order to achieve this goal, CSES-01 relies on nine instruments, operating on a Sun-synchronous polar orbit at ~500 km altitude, a 97° inclination, and a ~5-day revisiting periodicity. CSES-01 orbit allows for a detailed investigation of the high-latitude regions of the Earth — the ones more sensitive to the influence of the Sun, even though all payloads are switched off at ±65° of latitude, due to adjustments in altitude and additional scheduled maneuvers. This limitation was relaxed at the end of 2019 to allow the payloads to be active up to ±70° of latitude.

Among these payloads, the High-Energy Particle Detector (HEPD-01) was completely designed and built by the Italian Limadou Collaboration of the CSES mission. HEPD-01 is a light (~45 kg) and compact ($40.36 \times 53.00 \times 38.15$ cm^3) payload, optimized to measure electrons in the 3–100 MeV energy range and protons with kinetic energy between 30 and ~250 MeV, as well as light nuclei [19]. For this purpose, from top to bottom, the instrument is equipped with the following set of subdetectors: a tracker made up of two double-sided silicon microstrip planes ($213.2 \times 214.8 \times 0.3$ mm^3), a trigger system (T) including one EJ-200 plastic scintillator layer segmented into six paddles ($20 \times 3 \times 0.5$ cm^3 each), a range calorimeter comprising a tower of 16 plastic scintillator planes, P1, P2, ..., P16 ($15 \times 15 \times 1$ cm^3) and a matrix of 3×3 lutetium–yttrium oxyorthosilicate (LYSO) inorganic scintillator crystals ($5 \times 5 \times 4$ cm^3). Finally, the instrument is surrounded – laterally and at the bottom – by 5 plastic scintillators (VETO) in order to reject out-of-acceptance particles or particles which do not deposit all their energy inside the detector. Fig. 1 shows a schematic view of the detector. Thanks to this combination of subdetectors, HEPD-01 proved well suited to study the different particle populations along the CSES-01 orbit: galactic cosmic rays and their solar modulation [20,21], solar particles [22,23], trapped particles in the South Atlantic Anomaly [24,25], re-entrant albedo protons and electrons, presented respectively in [16] and in this work. Moreover, the detector was able to observe re-arrangements of the low-energy populations inside the Earth's magnetosphere due to geomagnetic storms [26,27].

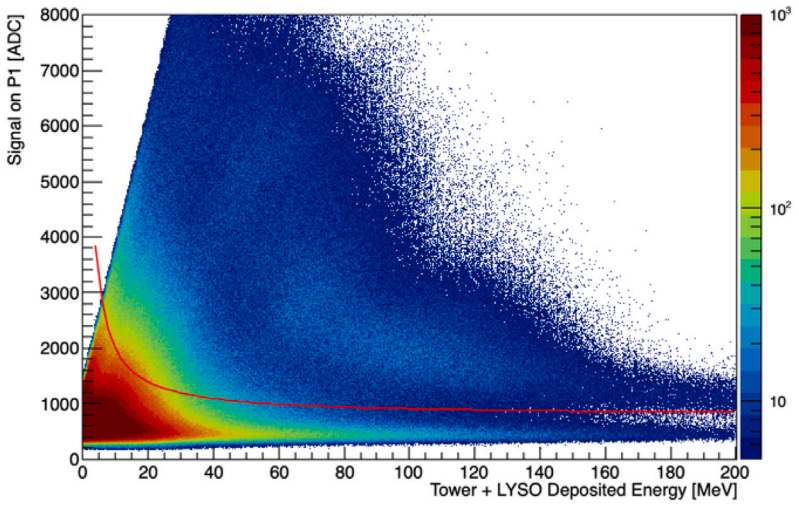

Fig. 2. Deposited signals by contained particles in plane P1 as a function of the total deposited energy inside the whole calorimeter (plastic scintillator tower and LYSO matrix). The red curve identifies the selection used in this analysis to discriminate electrons and positrons (population below the curve) from protons (population above the curve).

3. Data analysis

In order to calculate the re-entrant all-electron spectrum, we analyzed calibrated data in the period between August 1, 2018 and June 30, 2022 (for details on calibration procedure see [28]). During in-flight acquisition runs, an event is recorded if the impinging particle deposits a signal above the configured threshold in both the segmented trigger plane (T) and the first two planes of the plastic scintillator tower (P1 and P2). This trigger condition was set in July 2018 at the end of the commissioning phase, during which several onboard configurations and thresholds for the acquisition trigger were tested.

3.1. Event selection

An offline selection was applied at the data analysis level, to clean the sample as much as possible. In order to avoid multi-particle events and reduce secondaries generated in the upper portion of the payload, an event is considered valid if only one of the six paddles composing the trigger plane is hit. Moreover, only fully contained candidates (namely, particles stopping inside the plastic scintillator tower or the LYSO matrix) were included in the final sample: particles generating above-threshold signals in one of the 5 VETO planes were discarded. This condition ensures that the energy of the primary particle is entirely deposited inside the detector. Since the HEPD-01 entrance window points towards the zenith, the request of no signal in the bottom VETO plane also allows to discard the splash albedo component with an upward direction.

3.2. Electron/Positron identification

In order to discriminate electrons and positrons from protons, the most important source of background, the distribution of the deposited signal (in ADC counts) in the first scintillator plane (P1) as a function of the total deposited energy in the whole range calorimeter (tower + LYSO) was studied. Two separate populations can be identified in Fig. 2, which correspond to protons and electrons. The selection was made excluding all the events above the red curve, a function with the form $S(P1) = A/E_{dep} + B$, where A and B are fitted in order to obtain a selection efficiency of 90% for electrons and positrons in each energy interval. This curve was built using a Monte Carlo (MC) simulation of electrons with a flat energy distribution isotropically distributed.

The simulation software, developed by the Limadou Collaboration, is based on the Geant4 toolkit [29] and it includes the full event reconstruction, starting from the energy deposition inside the calorimeter sensitive volumes to the generation and propagation of the scintillation light produced in the calorimeter and its collection in the photomultiplier tubes (PMTs). This simulation was tuned with HEPD-01 beam test data (for further details see [28]).

3.3. Particles selection efficiency

The efficiency of the particle selections was assessed by using the digitized simulation described in the previous section. In particular, the distribution of the events passing the in-flight trigger, the containment and the electrons selection conditions, as described in Sections 3.1 and 3.2 was compared with the distribution of all events passing just the in-flight trigger and containment conditions. The particle selection efficiency was then estimated as a function of the deposited energy in the whole calorimeter (tower and LYSO). The result is a 90% efficiency on average on the whole energy interval. This efficiency is used to correct the number of selected particles to obtain an estimate of the true number of electrons fully contained in the calorimeter.

3.4. Orbital selections

In addition to the above-described set of selection criteria – used to obtain a clean sample of electrons – specific cuts were applied to select the re-entrant albedo component. As a first cut, particles were selected in the L-shell geomagnetic region between 1.1 and 1.2 R_E. Within HEPD-01 data, the L-shell, or McIlwain L-parameter, was calculated with a temporal precision of 1 s, considering the CSES-01 satellite position and using the IGRF-13 magnetospheric model [30] for the estimation of the Earth's magnetic field (B). At L-shell values between 1.1 and 1.2 R_E, a galactic electron needs to have an energy higher than 8 GeV to reach the detector location, while the request of particle containment inside the HEPD-01 calorimeter selects electrons with a maximum energy of ≃100 MeV. Consequently, all the fully-contained electrons selected in this L-shell region are secondaries produced in the atmosphere. Finally, we selected magnetic field values B > 23000 nT, in order to exclude the region corresponding to the South Atlantic Anomaly (SAA), where mostly trapped particles can be detected. Fig. 3 shows the counts of electrons and positrons as measured by HEPD-01 in the selection region.

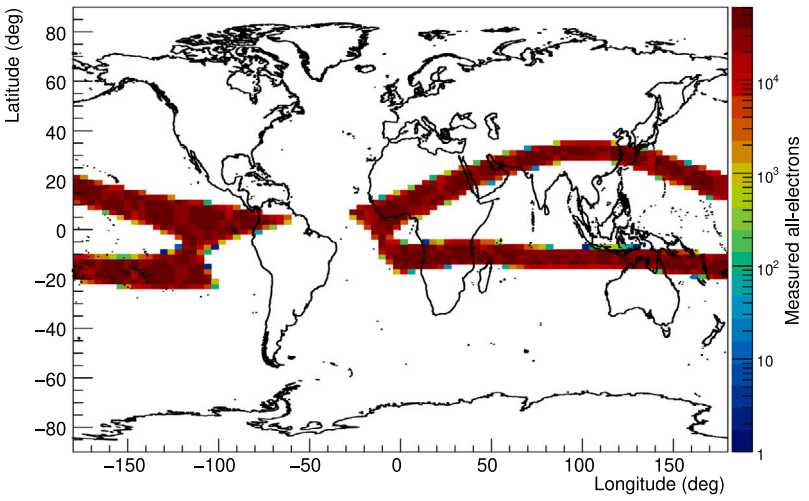

Fig. 3. All-electron counts in the selection region of L-shell between 1.1 and 1.2 R_E. Here all the selection cuts described in Sections 3.1 and 3.2 are applied.

3.5. Live time

The detector's live time is given by the time between the end of the processing of the previous event and the arrival of the current event, and corresponds to the time during which the detector is capable to acquire a new event. Its calculation is performed and managed by the trigger electronics board (for details see [31,32]). For this analysis, HEPD-01 was always considered sensitive to re-entrant electrons. Therefore, the live time was accumulated considering all the time spent by the apparatus in the orbital position selected by the aforementioned selection criteria (1.1 R_E < L-shell < 1.2 R_E and B > 23000 nT).

3.6. Energy statistical deconvolution (unfolding)

The re-entrant all-electron energy spectrum, thus measured as a function of the energy deposited in the entire calorimeter, was also corrected to account for particle slow down and energy loss in the trigger paddles and in the passive structures covering the sensitive materials of the apparatus. This correction was applied by means of an unfolding procedure, following the classical Bayesian approach proposed in [33, 34]. The detector response matrix or smearing matrix (see Fig. 4) – mapping the primary energy to the deposited energy in the calorimeter – was obtained by applying the previously described selections to a MC sample of electrons, isotropically distributed and simulated according to a power-law spectrum with index −1.1, compatible with the final spectrum obtained.

3.7. Geometrical factor

The geometrical factor of HEPD-01 is defined by the in-flight trigger condition and by the requirement of particle containment, as described in Section 3.1. It was evaluated by applying these conditions to a MC sample of isotropically generated electrons with a flat energy distribution. The distribution of the geometrical factor as a function of the electron primary particle energy is shown in Fig. 5.

The unfolded number of re-entrant electrons in each bin of primary energy is divided by the geometrical factor and live time of the detector.

3.8. Systematic uncertainties

The systematic uncertainties associated with the flux measurement can be identified to be both instrument- and procedure-related.

The main instrument-related uncertainty was identified in the selection cuts used to select a contained particle by the VETO system. To assess this uncertainty, the cuts – used to decide whether a VETO scintillator is hit by a particle – were increased and decreased by a factor 0.1 around their nominal value. The full spectrum was then re-evaluated and the relative difference between the nominal and varied spectra was used as systematic error.

As for procedure-related uncertainties, a source of systematics is related to the intrinsic accuracy of the employed unfolding technique. This was estimated by applying the unfolding algorithm to a Monte Carlo generated sample of electrons with the same characteristics of the one used to produce the smearing matrix. The relative difference between the primary particle energy spectrum and the unfolded one, averaged over the whole energy interval, was used as a systematic uncertainty for the procedure. An additional source of uncertainty is given by the geometrical factor calculation as described in Section 3.7. This systematic effect was assessed as the uncertainty given by the statistical power of the simulation dataset used for the determination of the geometrical factor. The event selection efficiency gives an additional systematic effect determined again from the statistical uncertainty in the estimation of the efficiency itself from the simulation sample. A systematic effect is also given by the mis-identification of protons as electrons. For this purpose, a Monte Carlo simulation was performed to reproduce the galactic and re-entrant proton spectrum – taken from literature – in the same L-shell region selected for this analysis. The proton contamination was thus evaluated from the relative counts of protons mis-tagged as electrons by the procedure described in Section 3.2. Finally, during the data-taking, a variation of the vetoes efficiency over time was observed. Although this was in part corrected by adding a varying threshold, a residual effect is still observable studying the counts distribution as a function of time. To account for this variation, an additional systematic uncertainty was added to the flux measurement, estimated as the maximum relative difference between counts on a 3-month interval basis (properly weighted with their live time).

Fig. 6 shows all the relative uncertainties, statistical and systematics, identified in the re-entrant all-electron measurement with the HEPD-01 detector, and their dependence on the electron energies. The total error, obtained by combining in quadrature the systematic uncertainties together and with the statistical uncertainty is also shown.

4. Results

The re-entrant all-electron differential spectrum $\Phi(E)$ was computed bin by bin as follows:

$$\Phi(E) = \frac{N_{unf}(E)}{GF(E) \times LT \times \Delta E}, \quad (1)$$

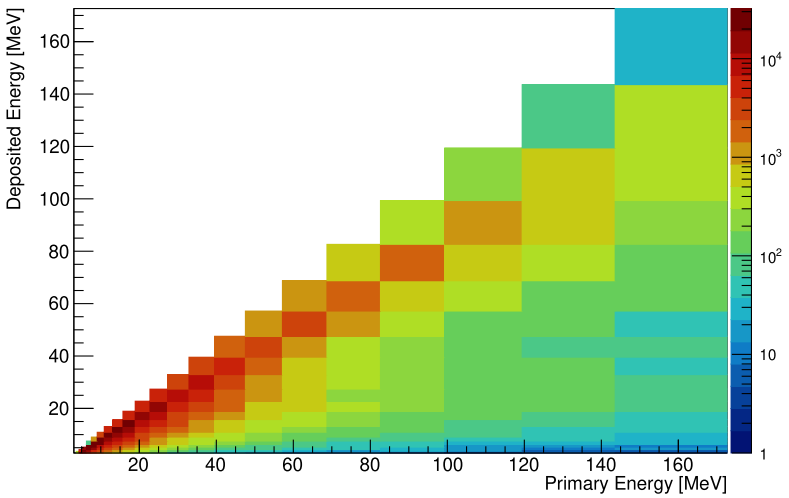

Fig. 4. The HEPD-01 detector response matrix, as obtained from a Monte Carlo simulation of electrons, with the primary and deposited energies on the x- and *y*-axis, respectively.

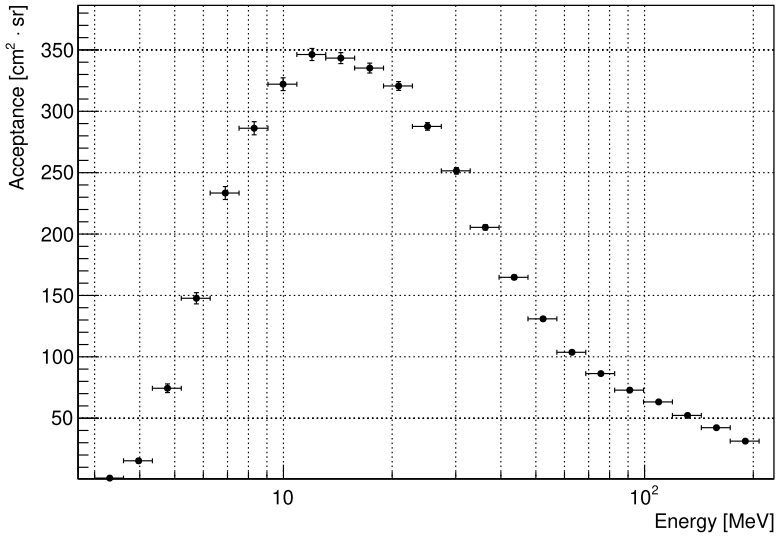

Fig. 5. Geometrical factor of the HEPD-01 detector as evaluated from the Monte Carlo distribution of the contained electrons (for details see text) normalized to the total number of primary events generated in the simulation. The error bars represent the statistical uncertainty.

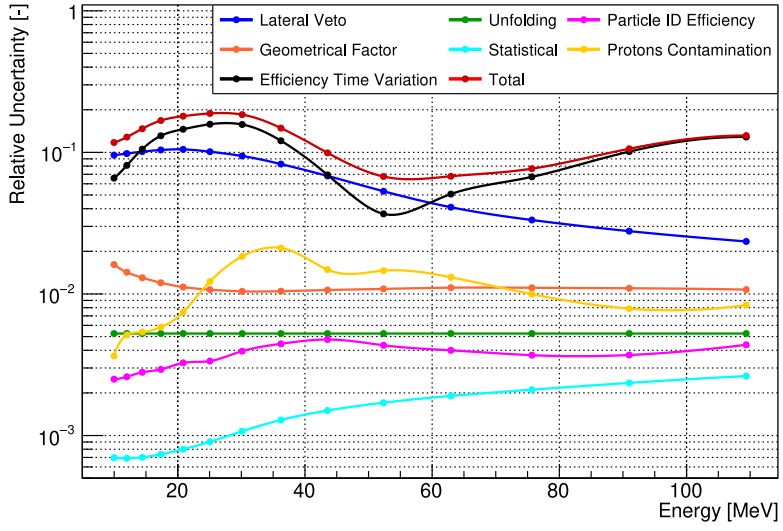

Fig. 6. Statistical and systematic sources of uncertainty, as a function of energy, which affect the HEPD-01 measurement of the re-entrant all-electron differential spectrum. The points are connected by a cubic spline.

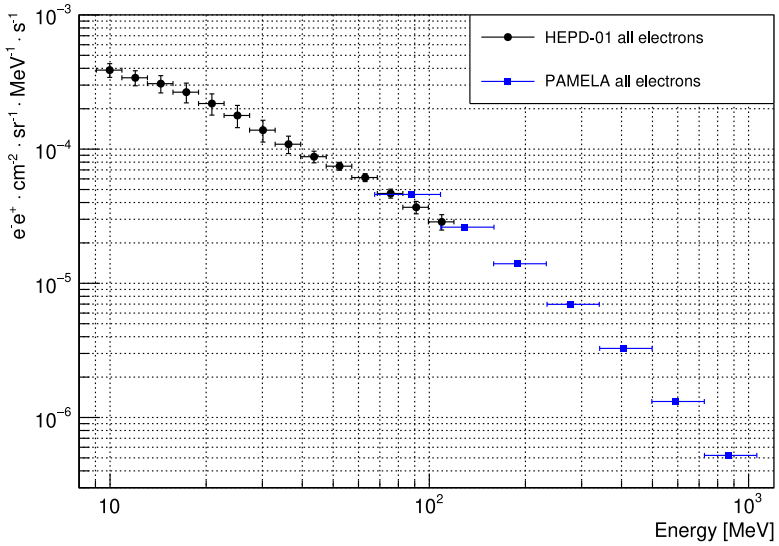

Fig. 7. Re-entrant all-electron differential spectrum measured by HEPD-01 (black) between 2018 and 2022 and compared with PAMELA (blue) data.

Table 1
Re-entrant all-electron fluxes measured by HEPD-01 shown in Fig. 7. The errors represent the total uncertainty associated to the flux measurement.

Kinetic energy [MeV]	Flux $[e^-e^+ \text{ cm}^{-2} \text{ sr}^{-1} \text{ MeV}^{-1} \text{ s}^{-1}]$
9.976 ± 0.916	$(3.876 \pm 0.455) \times 10^{-4}$
11.994 ± 1.102	$(3.395 \pm 0.435) \times 10^{-4}$
14.420 ± 1.324	$(3.067 \pm 0.451) \times 10^{-4}$
17.336 ± 1.592	$(2.648 \pm 0.444) \times 10^{-4}$
20.843 ± 1.914	$(2.182 \pm 0.393) \times 10^{-4}$
25.059 ± 2.301	$(1.787 \pm 0.337) \times 10^{-4}$
30.127 ± 2.767	$(1.394 \pm 0.258) \times 10^{-4}$
36.221 ± 3.327	$(1.096 \pm 0.163) \times 10^{-4}$
43.547 ± 4.000	$(8.781 \pm 0.871) \times 10^{-5}$
52.355 ± 4.809	$(7.349 \pm 0.496) \times 10^{-5}$
62.945 ± 5.781	$(6.094 \pm 0.413) \times 10^{-5}$
75.676 ± 6.950	$(4.700 \pm 0.361) \times 10^{-5}$
90.983 ± 8.356	$(3.624 \pm 0.384) \times 10^{-5}$
109.386 ± 10.046	$(2.805 \pm 0.369) \times 10^{-5}$

where each factor has been estimated as described in Section 3: $N_{unf}(E)$ represents the total number of re-entrant electrons, normalized by the selection efficiency and corrected by the unfolding procedure, $GF(E)$ is the geometrical factor, LT the live time, and ΔE the width of the energy bin. The resulting spectrum, as obtained by HEPD-01 in the period between August 1, 2018 and June 30, 2022, is shown in Fig. 7 (black) along with the PAMELA [35] (blue) measurement. The HEPD-01 spectrum points are listed in Table 1. PAMELA spectrum results from the sum of the re-entrant albedo electron and positron components, measured in the same L-shell region (between 1.1 and 1.2 R_E) of HEPD-01. It is important to stress the fact that the two measurements were performed in different periods of time: HEPD-01 data were taken in the solar minimum between the 24th and 25th cycles, while PAMELA ones cover the period 2006–2009 during the prolonged minimum of the 23rd solar cycle. Nevertheless, the agreement between the two spectra is quite good, assessing the substantial stability of re-entrant all-electrons over time. This is true because – at such low latitudes – the primary component responsible for the generation of the albedo populations is limited to rigidity greater than ~7 GV, which is affected by solar modulation, but it is not significant enough to be measured with our instrumentation, as shown in [36]. In support of this, Ref. [16] has already assessed the stability of the re-entrant proton population, resulting from the same mechanism producing the re-entrant electrons, during the HEPD-01 data-taking period.

5. Conclusions

In this work, we presented the measurement of the re-entrant all-electron spectrum in the energy range between 10 and ~100 MeV, performed by the HEPD-01 payload during the 2018–2022 period on board the CSES-01 satellite at Low-Earth orbit and at low-latitudes (L-shell = 1.1–1.2 R_E). Our results extend the previous PAMELA measurements towards a lower energy limit, where few recent experimental data are present. On the other hand, HEPD-01 could give new insights on the radiation environment near the Earth with unprecedented statistics and high stability in time. In turn, this could contribute to improve theoretical and empirical radiation models which continuously need new experimental data for validation purposes. Furthermore, this work confirms both the role and the capability of HEPD-01 in performing precise low-energy measurements of particle populations under the rigidity cutoff other than protons. Finally, these measurements will be soon performed even more precisely and in different conditions of the current solar cycle by the improved second High-Energy Particle Detector (HEPD-02), that has been launched on board the CSES-02 satellite on June 14th 2025. In particular with regard to electron measurements, the entire suite of onboard particle detectors (HEPD-02 and two Chinese instruments) will cover an extended energy range from tens of keV to hundreds of MeV, thus offering a further insight into the physics of re-entrant albedo particles throughout the 25th solar cycle.

CRediT authorship contribution statement

S. Amoroso: Software. **M. Babu:** Software. **S. Bartocci:** Software. **R. Battiston:** Supervision. **S. Beolè:** Resources. **W.J. Burger:** Software. **D. Campana:** Software. **P. Cipollone:** Resources. **L. Conti:** Software. **A. Contin:** Resources. **M. Cristoforetti:** Resources. **C. De Donato:** Resources. **C. De Santis:** Project administration. **A. Di Luca:** Resources. **F.M. Follega:** Software. **G. Gebbia:** Resources. **R. Iuppa:** Supervision. **A. Lega:** Resources. **M. Lolli:** Resources. **M. Martucci:** Writing – review & editing, Software. **G. Masciantonio:** Resources. **M. Mergè:** Software. **M. Mese:** Resources. **C. Neubüser:** Software. **R. Nicolaidis:** Software. **F. Nozzoli:** Resources. **A. Oliva:** Software. **G. Osteria:** Resources. **F. Palma:** Writing – review & editing. **B. Panico:** Software. **F. Perfetto:** Software. **A. Perinelli:** Resources. **P. Picozza:** Supervision. **S. Pietroni:** Software. **M. Pozzato:** Resources. **E. Ricci:** Resources. **L. Ricci:** Software. **M. Ricci:** Supervision. **S.B. Ricciarini:** Resources. **Z. Sahnoun:** Resources. **U. Savino:** Resources. **V. Scotti:** Resources. **M. Sorbara:** Writing – original draft, Software. **A. Sotgiu:** Software. **R. Sparvoli:** Supervision. **P. Ubertini:** Supervision. **V. Vilona:** Resources. **S. Zoffoli:** Supervision. **P. Zuccon:** Supervision.

Declaration of competing interest

The authors declare that they have no known competing financial interests or personal relationships that could have appeared to influence the work reported in this paper.

Acknowledgments

This work makes use of data from the CSES mission, a project funded by China National Space Administration (CNSA), China Earthquake Administration (CEA) in collaboration with the Italian Space Agency (ASI), National Institute for Nuclear Physics (INFN), Institute for Applied Physics (IFAC-CNR), and Institute for Space Astrophysics and Planetology (INAF-IAPS). This work was supported by the Italian Space Agency in the framework of the "Accordo Attuativo 2020-32.HH.0 Limadou Scienza+" (CUP F19C20000110005), the ASI-INFN Agreement No. n. 2014-037-R.0, addendum 2014-037-R-1-2017, and the ASI-INFN Agreement No. 2021-43-HH.0.

Data availability

The authors do not have permission to share data.

References

[1] S.B. Treiman, The Cosmic-Ray albedo, Phys. Rev. 91 (1953) 957–959, http://dx.doi.org/10.1103/PhysRev.91.957, URL https://link.aps.org/doi/10.1103/PhysRev.91.957.

[2] S.D. Verma, Measurement of the charged splash and re- entrant albedo of the cosmic radiation, J. Geophys. Res. 72 (1967) 915–925, URL https://api.semanticscholar.org/CorpusID:122795792.

[3] J.A.M. Bleeker, J.J. Burger, A. Scheepmaker, B.N. Swanenburg, Y. Tanaka, A balloon observation of high energy electrons, in: International Cosmic Ray Conference, in: International Cosmic Ray Conference, Vol. 1, 1965, p. 327.

[4] R.R. Daniel, S.A. Stephens, Electron component of the primary cosmic radiation at energies >15 GeV, Phys. Rev. Lett. 15 (1965) 769–772, http://dx.doi.org/10.1103/PhysRevLett.15.769, URL https://link.aps.org/doi/10.1103/PhysRevLett.15.769.

[5] J.W. Schmoker, J.A. Earl, Magnetic-Cloud-Chamber observations of Low-Energy Cosmic-Ray electrons, Phys. Rev. 138 (1965) B300–B302, http://dx.doi.org/10.1103/PhysRev.138.B300, URL https://link.aps.org/doi/10.1103/PhysRev.138.B300.

[6] K.P. Wenzel, E.C. Stone, R.E. Vogt, Splash albedo protons between 4 and 315 MeV at high and low geomagnetic latitudes, J. Geophys. Res. 80 (25) (1975) 3580, http://dx.doi.org/10.1029/JA080i025p03580.

[7] O. Adriani, G. Barbarino, G. Bazilevskaya, R. Bellotti, M. Boezio, E. Bogomolov, M. Bongi, V. Bonvicini, S. Bottai, A. Bruno, F. Cafagna, D. Campana, R. Carbone, P. Carlson, M. Casolino, G. Castellini, M. De Pascale, C. De Santis, N. De Simone, V. Di Felice, V. Formato, A. Galper, U. Giaccari, A. Karelin, M. Kheymits, S. Koldashov, S. Koldobskiy, S. Krut'kov, A. Kvashnin, A. Leonov, V. Malakhov, L. Marcelli, M. Martucci, A. Mayorov, W. Menn, V. Mikhailov, E. Mocchiutti, A. Monaco, N. Mori, R. Munini, N. Nikonov, G. Osteria, P. Papini, M. Pearce, P. Picozza, C. Pizzolotto, M. Ricci, S. Ricciarini, L. Rossetto, R. Sarkar, M. Simon, R. Sparvoli, P. Spillantini, Y. Stozhkov, A. Vacchi, E. Vannuccini, G. Vasilyev, S. Voronov, J. Wu, Y. Yurkin, G. Zampa, N. Zampa, V. Zverev, The PAMELA Mission: Heralding a new era in precision cosmic ray physics, Phys. Rep. 544 (4) (2014) 323–370, http://dx.doi.org/10.1016/j.physrep.2014.06.003, URL https://www.sciencedirect.com/science/article/pii/S0370157314002087, The PAMELA Mission: Heralding a new era in precision cosmic ray physics.

[8] S. Voronov, A.M. Galper, S.V. Koldashov, L.V. Maslennikov, V.V. Mikhailov, A.V. Popov, Cosm. Res. Engl. Transl. 30 (1) (1992) 140.

[9] E. Fiandrini, G. Esposito, B. Bertucci, B. Alpat, R. Battiston, W. Burger, G. Lamanna, P. Zuccon, Leptons with $E > 200$ MeV trapped in the earth's radiation belts, J. Geophys. Res. Atmos. 107 (2001) http://dx.doi.org/10.1029/2001JA900151.

[10] M. Aguilar, J. Alcaraz, J. Allaby, B. Alpat, G. Ambrosi, H. Anderhub, L. Ao, A. Arefiev, P. Azzarello, E. Babucci, L. Baldini, M. Basile, D. Barancourt, F. Barao, G. Barbier, G. Barreira, R. Battiston, R. Becker, U. Becker, L. Bellagamba, P. Bn, J. Berdugo, P. Berges, B. Bertucci, A. Biland, S. Bizzaglia, S. Blasko, G. Boella, M. Boschini, M. Bourquin, L. Brocco, G. Bruni, M. Bunerd, J. Burger, W. Burger, X. Cai, C. Camps, P. Cannarsa, M. Capell, D. Casadei, J. Casaus, G. Castellini, C. Cecchi, Y. Chang, H. Chen, H. Chen, Z. Chen, N. Chernoplekov, T. Chiueh, K. Cho, M. Choi, Y. Choi, Y. Chuang, F. Cindolo, V. Commichau, A. Contin, E. Cortina-Gil, M. Cristinziani, J. da Cunha, T. Dai, C. Delgado, J. Deus, N. Dinu, L. Djambazov, I. D'Antone, Z. Dong, P. Emonet, J. Engelberg, F. Eppling, T. Eronen, G. Esposito, P. Extermann, J. Favier, E. Fiandrini, P. Fisher, G. Fluegge, N. Fouque, Y. Galaktionov, M. Gervasi, P. Giusti, D. Grandi, O. Grimms, W. Gu, K. Hangarter, A. Hasan, V. Hermel, H. Hofer, M. Huang, W. Hungerford, M. Ionica, R. Ionica, M. Jongmanns, K. Karlamaa, W. Karpinski, G. Kenney, J. Kenny, D. Kim, G. Kim, K. Kim, M. Kim, A. Klimentov, R. Kossakowski, V. Koutsenko, M. Kraeber, G. Laborie, T. Laitinen, G. Lamanna, E. Lanciotti, G. Laurenti, A. Lebedev, C. Lechanoine-Leluc, M. Lee, S. Lee, G. Levi, P. Levtchenko, C. Liu, H. Liu, I. Lopes, G. Lu, Y. Lu, K. Lbelsmeyer, D. Luckey, W. Lustermann, C. Maa, A. Margotti, F. Mayet, R. McNeil, B. Meillon, M. Menichelli, A. Mihul, A. Mourao, A. Mujunen, F. Palmonari, A. Papi, H. Park, W. Park, M. Pauluzzi, F. Pauss, E. Perrin, A. Pesci, A. Pevsner, M. Pimenta, V. Plyaskin, V. Pojidaev, M. Pohl, V. Postolache, N. Produit, P. Rancoita, D. Rapin, F. Raupach, D. Ren, Z. Ren, M. Ribordy, J. Richeux, E. Riihonen, J. Ritakari, S. Ro, U. Roeser, C. Rossin, R. Sagdeev, D. Santos, G. Sartorelli, C. Sbarra, S. Schael, A. Schultz von Dratzig, G. Schwering, G. Scolieri, E. Seo, J. Shin, V. Shoutko, E. Shoumilov, R. Siedling, D. Son, T. Song, M. Steuer, G. Sun, H. Suter, X. Tang, S.C. Ting, S. Ting, M. Tornikoski, J. Torsti, J. Trmper, J. Ulbricht, S. Urpo, E. Valtonen, J. Vandenhirtz, F. Velcea, E. Velikhov, B. Verlaat, I. Vetlitsky, F. Vezzu, J. Vialle, G. Viertel, D. Vit, H. Gunten, S. Wicki, W. Wallraff, B. Wang, J. Wang, Y. Wang, K. Wiik, C. Williams, S. Wu, P. Xia, J. Yan, L. Yan, C. Yang, J. Yang, M. Yang, S. Ye, P. Yeh, Z. Xu, H. Zhang, Z. Zhang, D. Zhao, G. Zhu, W. Zhu, H. Zhuang, A. Zichichi, B. Zimmermann, P. Zuccon, The alpha magnetic spectrometer (AMS) on the international space station: Part I results from the test flight on the space shuttle, Phys. Rep. 366 (6) (2002) 331–405, http://dx.doi.org/10.1016/S0370-1573(02)00013-3, URL https://www.sciencedirect.com/science/article/pii/S0370157302000133.

[11] Pamela Collaboration, O. Adriani, G.C. Barbarino, G.A. Bazilevskaya, R. Bellotti, M. Boezio, E.A. Bogomolov, M. Bongi, V. Bonvicini, S. Bottai, A. Bruno, F. Cafagna, D. Campana, P. Carlson, M. Casolino, G. Castellini, C. de Santis, V. di Felice, A.M. Galper, A.V. Karelin, S.V. Koldashov, S. Koldobskiy, S.Y. Krutkov, A.N. Kvashnin, A. Leonov, V. Malakhov, L. Marcelli, M. Martucci, A.G. Mayorov, W. Menn, M. Mergè, V.V. Mikhailov, E. Mocchiutti, A. Monaco, R. Munini, N. Mori, G. Osteria, B. Panico, P. Papini, M. Pearce, P. Picozza, M. Ricci, S.B. Ricciarini, M. Simon, R. Sparvoli, P. Spillantini, Y.I. Stozhkov, A. Vacchi, E. Vannuccini, G. Vasilyev, S.A. Voronov, Y.T. Yurkin, G. Zampa, N. Zampa, Ten years of PAMELA in space, Nuovo Cimento Riv. Ser. 40 (10) (2017) 473–522, http://dx.doi.org/10.1393/ncr/i2017-10140-x.

[12] S. Mechbal, P.-S. Mangeard, J.M. Clem, P.A. Evenson, R.P. Johnson, B. Lucas, J. Roth, Measurement of Low-energy Cosmic-Ray electron and positron spectra at 1 au with the AESOP-Lite spectrometer, Astrophys. J. 903 (1) (2020) 21, http://dx.doi.org/10.3847/1538-4357/abb46f.

[13] S. Martin, B. Lucas, P.S. Mangeard, J. Roth, J.M. Clem, P. Evenson, R. Johnson, Geomagnetic diurnal transitions of positron and electron flux at 20 - 300MeV as observed by the AESOP-Lite Balloon Payload, in: 38th International Cosmic Ray Conference, 2024, p. 1329.

[14] S.V. Koldashov, V.V. Mikhailov, S.A. Voronov, Electron and positron Albedo spectra with energy more than 20 MeV, in: International Cosmic Ray Conference, in: International Cosmic Ray Conference, Vol. 4, 1995, p. 993.

[15] L. Derome, M. Buénerd, Y. Liu, Secondary electrons and positrons in near earth orbit, Phys. Lett. B 515 (1) (2001) 1–5, http://dx.doi.org/10.1016/S0370-2693(01)00832-2, URL https://www.sciencedirect.com/science/article/pii/S0370269301008322.

[16] M. Martucci, A. Oliva, R. Battiston, S. Beolè, P. Cipollone, A. Contin, M. Cristoforetti, C. De Donato, C. De Santis, A. Di Luca, F. Follega, G. Gebbia, R. Iuppa, A. Lega, M. Lolli, G. Masciantonio, M. Mese, C. Neubüser, R. Nicolaidis, F. Nozzoli, G. Osteria, F. Palma, B. Panico, F. Perfetto, A. Perinelli, P. Picozza, E. Ricci, M. Ricci, S. Ricciarini, Z. Sahnoun, U. Savino, V. Scotti, M. Sorbara, A. Sotgiu, R. Sparvoli, P. Ubertini, V. Vilona, S. Zoffoli, P. Zuccon, Measurements of low-energy, re-entrant albedo protons by the HEPD-01 space-borne detector, Astropart. Phys. 162 (2024) 102993, http://dx.doi.org/10.1016/j.astropartphys.2024.102993, URL https://www.sciencedirect.com/science/article/pii/S0927650524000707.

[17] C. De Santis, S. Ricciarini, The High Energy Particle Detector (HEPD-02) for the second China seismo-electromagnetic satellite (CSES-02), in: Proceedings of 37th International Cosmic Ray Conference — PoS(ICRC2021), Vol. 395, 2021, p. 058, http://dx.doi.org/10.22323/1.395.0058.

[18] X. Shen, et al., The state-of-the-art of the China Seismo-Electromagnetic satellite mission, Sci. China Technol. Sci. 61 (5) (2018) 634, http://dx.doi.org/10.1007/s11431-018-9242-0.

[19] P. Picozza, R. Battiston, G. Ambrosi, S. Bartocci, L. Basara, W.J. Burger, D. Campana, L. Carfora, M. Casolino, G. Castellini, P. Cipollone, L. Conti, A. Contin, C. De Donato, C. De Santis, F.M. Follega, C. Guandalini, M. Ionica, R. Iuppa, G. Laurenti, I. Lazzizzera, M. Lolli, C. Manea, L. Marcelli, M. Martucci, G. Masciantonio, M. Mergé, G. Osteria, L. Pacini, F. Palma, F. Palmonari, B. Panico, A. Parmentier, L. Patrizii, F. Perfetto, M. Piersanti, M. Pozzato, M. Puel, I. Rashevskaya, E. Ricci, M. Ricci, S. Ricciarini, V. Scotti, A. Sotgiu, R. Sparvoli, B. Spataro, V. Vitale, P. Zuccon, S. Zoffoli, Scientific goals and in-orbit performance of the high-energy particle detector on board the CSES, Astrophys. J. Suppl. 243 (1) (2019) 16, http://dx.doi.org/10.3847/1538-4365/ab276c.

[20] S. Bartocci, R. Battiston, W.J. Burger, D. Campana, L. Carfora, G. Castellini, L. Conti, A. Contin, C.D. Donato, F.D. Persio, C.D. Santis, P. Diego, F.M. Follega, R. Iuppa, I. Lazzizzera, N. Marcelli, M. Martucci, G. Masciantonio, M. Mergé, G. Osteria, F. Palma, F. Palmonari, A. Parmentier, F. Perfetto, P. Picozza, M. Piersanti, M. Pozzato, I. Rashevskaya, E. Ricci, M. Ricci, S. Ricciarini, V. Scotti, A. Sotgiu, R. Sparvoli, P. Ubertini, V. Vitale, S. Zoffoli, P. Zuccon, Galactic Cosmic-Ray hydrogen spectra in the 40–250 MeV range measured by the High-Energy particle detector (HEPD) on board the CSES-01 Satellite between 2018 and 2020, Astrophys. J. 901 (1) (2020) 8, http://dx.doi.org/10.3847/1538-4357/abad3e.

[21] M. Martucci, R. Ammendola, D. Badoni, S. Bartocci, R. Battiston, S. Beolè, W.J. Burger, D. Campana, G. Castellini, P. Cipollone, S. Coli, L. Conti, A. Contin, M. Cristoforetti, G. D'Angelo, C.D. Donato, C.D. Santis, A. Di Luca, F.M. Follega, G. Gebbia, R. Iuppa, A. Lega, M. Lolli, N. Marcelli, G. Masciantonio, M. Merg, M. Mese, C. Neubüser, F. Nozzoli, A. Oliva, G. Osteria, L. Pacini, F. Palma, F. Palmonari, B. Panico, A. Parmentier, S. Perciballi, F. Perfetto, P. Picozza, M. Pozzato, G.M. Rebustini, E. Ricci, M. Ricci, S.B. Ricciarini, U. Savino, Z. Sahnoun, V. Scotti, A. Sotgiu, R. Sparvoli, P. Ubertini, V. Vilona, V. Vitale, S. Zoffoli, P. Zuccon, O.P.M. Aslam, M.D. Ngobeni, M.S. Potgieter, Time dependence of 50–250 MeV galactic Cosmic-Ray protons between solar cycles 24 and 25, measured by the High-energy particle detector on board the CSES-01 satellite, Astrophys. J. Lett. 945 (2) (2023) L39, http://dx.doi.org/10.3847/2041-8213/acbea7.

[22] M. Martucci, M. Laurenza, S. Benella, F. Berrilli, D. Del Moro, L. Giovannelli, A. Parmentier, M. Piersanti, G. Albrecht, S. Bartocci, R. Battiston, W.J. Burger, D. Campana, L. Carfora, G. Consolini, L. Conti, A. Contin, C. De Donato, C. De Santis, F.M. Follega, R. Iuppa, A. Lega, N. Marcelli, G. Masciantonio, M. Merg, M. Mese, A. Oliva, G. Osteria, F. Palma, B. Panico, F. Perfetto, P. Picozza, M. Pozzato, E. Ricci, M. Ricci, S.B. Ricciarini, Z. Sahnoun, V. Scotti, A. Sotgiu, R. Sparvoli, V. Vitale, S. Zoffoli, P. Zuccon, The first Ground-Level enhancement of solar cycle 25 as seen by the High-Energy particle detector (HEPD-01) on board the CSES-01 satellite, Space Weather. 21 (1) (2023) e2022SW003191, http://dx.doi.org/10.1029/2022SW003191, arXiv:https://agupubs.onlinelibrary.wiley.com/doi/pdf/10.1029/2022SW003191 URL https://agupubs.onlinelibrary.wiley.com/doi/abs/10.1029/2022SW003191, e2022SW003191 2022SW003191.

[23] S. Bartocci, R. Battiston, S. Benella, S. Beolè, W.J. Burger, P. Cipollone, A. Contin, M. Cristoforetti, C.D. Donato, C.D. Santis, A. Di Luca, F.M. Follega, G. Gebbia, R. Iuppa, M. Laurenza, A. Lega, M. Lolli, M. Martucci, G. Masciantonio, M. Mergè, M. Mese, C. Neubüser, R. Nicolaidis, F. Nozzoli, A. Oliva, G. Osteria, F. Palma, B. Panico, F. Perfetto, A. Perinelli, P. Picozza, E. Ricci, M. Ricci, S.B. Ricciarini, Z. Sahnoun, U. Savino, V. Scotti, M. Sorbara, A. Sotgiu, R. Sparvoli, P. Ubertini, V. Vilona, S. Zoffoli, P. Zuccon, Multispacecraft observations of protons and helium nuclei in some solar energetic particle events towards the maximum of cycle 25, Astrophys. J. 974 (2) (2024) 176, http://dx.doi.org/10.3847/1538-4357/ad7395.

[24] M. Martucci, S. Bartocci, R. Battiston, D. Campana, L. Carfora, L. Conti, A. Contin, C. De Donato, C. De Santis, F. Follega, R. Iuppa, N. Marcelli, G. Masciantonio, M. Merg, A. Oliva, G. Osteria, F. Palma, A. Parmentier, F. Perfetto, P. Picozza, M. Pozzato, E. Ricci, M. Ricci, S. Ricciarini, Z. Sahnoun, V. Scotti, A. Sotgiu, R. Sparvoli, V. Vitale, S. Zoffoli, P. Zuccon, CSES-Limadou Collaboration, New results on protons inside the South Atlantic Anomaly, at energies between 40-250 MeV in the period 2018–2020, from the CSES-01 satellite mission, Phys. Rev. D 105 (6) (2022) http://dx.doi.org/10.1103/PhysRevD.105.062001, URL https://www.scopus.com/inward/record.uri?eid=2-s2.0-85126968787&doi=10.1103%2fPhysRevD.105.062001&partnerID=40&md5=266cfd12f128ab41e4a3a0dd796ed629.

[25] S. Bartocci, R. Battiston, S. Beolè, W.J. Burger, D. Campana, P. Cipollone, A. Contin, M. Cristoforetti, C. De Donato, C. De Santis, A. Di Luca, F.M. Follega, G. Gebbia, R. Iuppa, A. Lega, M. Lolli, M. Martucci, G. Masciantonio, M. Mergè, M. Mese, C. Neubüser, R. Nicolaidis, F. Nozzoli, A. Oliva, G. Osteria, F. Palma, B. Panico, F. Perfetto, A. Perinelli, P. Picozza, E. Ricci, L. Ricci, M. Ricci, S.B. Ricciarini, Z. Sahnoun, U. Savino, V. Scotti, M. Sorbara, A. Sotgiu, R. Sparvoli, P. Ubertini, V. Vilona, S. Zoffoli, P. Zuccon, CSES-Limadou Collaboration, Mapping the south atlantic anomaly charged particle environment with the HEPD-01 detector on board the CSES-01 satellite, Phys. Rev. D 111 (2025) 022001, http://dx.doi.org/10.1103/PhysRevD.111.022001, URL https://link.aps.org/doi/10.1103/PhysRevD.111.022001.

[26] F. Palma, A. Sotgiu, A. Parmentier, M. Martucci, M. Piersanti, S. Bartocci, R. Battiston, W.J. Burger, D. Campana, L. Carfora, G. Castellini, L. Conti, A. Contin, G. D'Angelo, C. De Donato, C. De Santis, F.M. Follega, R. Iuppa, I. Lazzizzera, N. Marcelli, G. Masciantonio, M. Merg, A. Oliva, G. Osteria, F. Palmonari, B. Panico, F. Perfetto, P. Picozza, M. Pozzato, E. Ricci, M. Ricci, S.B. Ricciarini, Z. Sahnoun, V. Scotti, R. Sparvoli, V. Vitale, S. Zoffoli, P. Zuccon, The august 2018 geomagnetic storm observed by the High-Energy particle detector on board the CSES-01 satellite, Appl. Sci. 11 (12) (2021) http://dx.doi.org/10.3390/app11125680, URL https://www.mdpi.com/2076-3417/11/12/5680.

[27] M. Piersanti, D. Del Moro, A. Parmentier, M. Martucci, F. Palma, A. Sotgiu, C. Plainaki, G. D'Angelo, F. Berrilli, D. Recchiuti, E. Papini, L. Giovannelli, G. Napoletano, R. Iuppa, P. Diego, A. Cicone, M. Merg, C. De Donato, C. De Santis, R. Sparvoli, P. Ubertini, R. Battiston, P. Picozza, On the Magnetosphere-Ionosphere coupling during the May 2021 geomagnetic storm, Space Weather. 20 (6) (2022) e2021SW003016, http://dx.doi.org/10.1029/2021SW003016, arXiv:https://agupubs.onlinelibrary.wiley.com/doi/pdf/10.1029/2021SW003016 URL https://agupubs.onlinelibrary.wiley.com/doi/abs/10.1029/2021SW003016, e2021SW003016 2021SW003016.

[28] G. Ambrosi, S. Bartocci, L. Basara, R. Battiston, W. Burger, D. Campana, L. Carfora, G. Castellini, P. Cipollone, L. Conti, A. Contin, C. De Donato, F. De Persio, C. De Santis, F. Follega, C. Guandalini, M. Ionica, R. Iuppa, G. Laurenti, I. Lazzizzera, M. Lolli, C. Manea, M. Martucci, G. Masciantonio, M. Merg, G. Osteria, L. Pacini, F. Palma, F. Palmonari, B. Panico, A. Parmentier, L. Patrizii, F. Perfetto, P. Picozza, M. Piersanti, M. Pozzato, M. Puel, I. Rashevskaya, E. Ricci, M. Ricci, S. Ricciarini, V. Scotti, A. Sotgiu, R. Sparvoli, B. Spataro, V. Vitale, S. Zoffoli, P. Zuccon, Beam test calibrations of the HEPD detector on board the China seismo-electromagnetic satellite, Nucl. Instrum. Methods Phys. Res. A 974 (2020) 164170, http://dx.doi.org/10.1016/j.nima.2020.164170, URL http://www.sciencedirect.com/science/article/pii/S0168900220305660.

[29] S. Agostinelli, J. Allison, K. Amako, J. Apostolakis, H. Araujo, P. Arce, M. Asai, D. Axen, S. Banerjee, G. Barrand, F. Behner, L. Bellagamba, J. Boudreau, L. Broglia, A. Brunengo, H. Burkhardt, S. Chauvie, J. Chuma, R. Chytracek, G. Cooperman, G. Cosmo, P. Degtyarenko, A. Dell'Acqua, G. Depaola, D. Dietrich, R. Enami, A. Feliciello, C. Ferguson, H. Fesefeldt, G. Folger, F. Foppiano, A. Forti, S. Garelli, S. Giani, R. Giannitrapani, D. Gibin, J. Gómez Cadenas, I. González, G. Gracia Abril, G. Greeniaus, W. Greiner, V. Grichine, A. Grossheim, S. Guatelli, P. Gumplinger, R. Hamatsu, K. Hashimoto, H. Hasui, A. Heikkinen, A. Howard, V. Ivanchenko, A. Johnson, F. Jones, J. Kallenbach, N. Kanaya, M. Kawabata, Y. Kawabata, M. Kawaguti, S. Kelner, P. Kent, A. Kimura, T. Kodama, R. Kokoulin, M. Kossov, H. Kurashige, E. Lamanna, T. Lampén, V. Lara, V. Lefebure, F. Lei, M. Liendl, W. Lockman, F. Longo, S. Magni, M. Maire, E. Medernach, K. Minamimoto, P. Mora de Freitas, Y. Morita, K. Murakami, M. Nagamatu, R. Nartallo, P. Nieminen, T. Nishimura, K. Ohtsubo, M. Okamura, S. O'Neale, Y. Oohata, K. Paech, J. Perl, A. Pfeiffer, M. Pia, F. Ranjard, A. Rybin, S. Sadilov, E. Di Salvo, G. Santin, T. Sasaki, N. Savvas, Y. Sawada, S. Scherer, S. Sei, V. Sirotenko, D. Smith, N. Starkov, H. Stoecker, J. Sulkimo, M. Takahata, S. Tanaka, E. Tcherniaev, E. Safai Tehrani, M. Tropeano, P. Truscott, H. Uno, L. Urban, P. Urban, M. Verderi, A. Walkden, W. Wander, H. Weber, J. Wellisch, T. Wenaus, D. Williams, D. Wright, T. Yamada, H. Yoshida, D. Zschiesche, Geant4—a simulation toolkit, Nucl. Instrum. Methods Phys. Res. Sect. A: Accel. Spectrometers Detect. Assoc. Equip. 506 (3) (2003) 250–303, http://dx.doi.org/10.1016/S0168-9002(03)01368-8, URL https://www.sciencedirect.com/science/article/pii/S0168900203013688.

[30] P. Alken, E. Thébault, C.D. Beggan, H. Amit, J. Aubert, J. Baerenzung, T.N. Bondar, W.J. Brown, S. Califf, A. Chambodut, A. Chulliat, G.A. Cox, C.C. Finlay, A. Fournier, N. Gillet, A. Grayver, M.D. Hammer, M. Holschneider, L. Huder, G.G. Hulot, T. Jager, C. Kloss, M. Korte, W. Kuang, A. Kuvshinov, B. Langlais, J.-M. Léger, V. Lesur, P.W. Livermore, F.J. Lowes, S. Macmillan, W. Magnes, M. Mandea, S. Marsal, J. Matzka, M.C. Metman, T. Minami, A. Morschhauser, J.E. Mound, M. Nair, S. Nakano, N. Olsen, F.J. Pavón-Carrasco, V.G. Petrov, G. Ropp, M. Rother, T.J. Sabaka, S. Sanchez, D. Saturnino, N.R. Schnepf, X. Shen, C. Stolle, A. Tangborn, L. Tøffner-Clausen, H. Toh, J.M. Torta, J. Varner, F. Vervelidou, P. Vigneron, I. Wardinski, J. Wicht, A. Woods, Y. Yang, Z. Zeren, B. Zhou, International geomagnetic reference field: the thirteenth generation,

Earth Planets Space 73 (2021) 49, http://dx.doi.org/10.1186/s40623-020-01288-x, URL https://cea.hal.science/cea-03141089.

[31] A. Sotgiu, C. De Donato, C. Fornaro, S. Tassa, M. Scannavini, D. Iannaccio, G. Ambrosi, S. Bartocci, L. Basara, R. Battiston, W.J. Burger, D. Campana, L. Carfora, G. Castellini, P. Cipollone, L. Conti, A. Contin, F. De Persio, C. De Santis, F.M. Follega, C. Guandalini, M. Ionica, R. Iuppa, G. Laurenti, I. Lazzizzera, M. Lolli, C. Manea, M. Martucci, G. Masciantonio, M. Mergé, G. Osteria, L. Pacini, F. Palma, F. Palmonari, B. Panico, A. Parmentier, F. Perfetto, P. Picozza, M. Piersanti, M. Pozzato, M. Puel, I. Rashevskaya, E. Ricci, M. Ricci, S.B. Ricciarini, V. Scotti, R. Sparvoli, B. Spataro, V. Vitale, S. Zoffoli, P. Zuccon, Control and data acquisition software of the High-Energy particle detector on board the China Seismo-Electromagnetic satellite space mission, Softw.: Pr. Exp. (2020) 1–22, http://dx.doi.org/10.1002/spe.2947, arXiv:https://onlinelibrary.wiley.com/doi/pdf/10.1002/spe.2947 URL https://onlinelibrary.wiley.com/doi/abs/10.1002/spe.2947.

[32] G. Ambrosi, S. Bartocci, L. Basara, R. Battiston, W. Burger, D. Campana, M. Caprai, L. Carfora, G. Castellini, P. Cipollone, L. Conti, A. Contin, C. De Donato, F. De Persio, C. De Santis, F. Follega, C. Guandalini, G. Gebbia, M. Ionica, R. Iuppa, G. Laurenti, I. Lazzizzera, M. Lolli, C. Manea, M. Martucci, G. Masciantonio, M. Merg, M. Mese, G. Osteria, L. Pacini, F. Palma, F. Palmonari, B. Panico, A. Parmentier, L. Patrizii, F. Perfetto, P. Picozza, M. Pozzato, M. Puel, I. Rashevskaya, E. Ricci, M. Ricci, S. Ricciarini, Z. Sahnoun, V. Scotti, A. Sotgiu, R. Sparvoli, V. Vitale, S. Zoffoli, P. Zuccon, The electronics of the High-Energy particle detector on board the CSES-01 satellite, Nucl. Instrum. Methods. Phys. Res. A 1013 (2021) 165639, http://dx.doi.org/10.1016/j.nima.2021.165639, URL https://www.sciencedirect.com/science/article/pii/S0168900221006240.

[33] G. D'Agostini, A multidimensional unfolding method based on Bayes' theorem, Nucl. Instrum. Methods Phys. Res. A 362 (2) (1995) 487–498, http://dx.doi.org/10.1016/0168-9002(95)00274-X.

[34] G. D'Agostini, Improved iterative Bayesian unfolding, in: Alliance Workshop on Unfolding and Data Correction, 2010, arXiv:1010.0632.

[35] L. Grishantseva, O. Adriani, G. Barbarino, G. Bazilevskaya, R. Bellotti, M. Boezio, E. Bogomolov, L. Bonechi, M. Bongi, V. Bonvicini, S. Borisov, S. Bottai, A. Bruno, F. Cafagna, D. Campana, P. Carlson, M. Casolino, G. Castellini, M. Pascale, V. Zverev, Sub-cutoff electrons and positrons in the near Earth space, in: 31st International Cosmic Ray Conference, ICRC 2009, 2009.

[36] M. Martucci, R. Munini, M. Boezio, V.D. Felice, O. Adriani, G.C. Barbarino, G.A. Bazilevskaya, R. Bellotti, M. Bongi, V. Bonvicini, S. Bottai, A. Bruno, F. Cafagna, D. Campana, P. Carlson, M. Casolino, G. Castellini, C.D. Santis, A.M. Galper, A.V. Karelin, S.V. Koldashov, S. Koldobskiy, S.Y. Krutkov, A.N. Kvashnin, A. Leonov, V. Malakhov, L. Marcelli, N. Marcelli, A.G. Mayorov, W. Menn, M. Mergè, V.V. Mikhailov, E. Mocchiutti, A. Monaco, N. Mori, G. Osteria, B. Panico, P. Papini, M. Pearce, P. Picozza, M. Ricci, S.B. Ricciarini, M. Simon, R. Sparvoli, P. Spillantini, Y.I. Stozhkov, A. Vacchi, E. Vannuccini, G. Vasilyev, S.A. Voronov, Y.T. Yurkin, G. Zampa, N. Zampa, M.S. Potgieter, J.L. Raath, Proton fluxes measured by the PAMELA experiment from the minimum to the maximum solar activity for solar cycle 24, Astrophys. J. Lett. 854 (1) (2018) L2, http://dx.doi.org/10.3847/2041-8213/aaa9b2.